Survey of Materials for Nanoskiving and Influence of the Cutting Process on the Nanostructures Produced

Darren J. Lipomi, Ramses V. Martinez, Robert M. Rioux, Ludovico Cademartiri, William F. Reus, and George M. Whitesides*

Department of Chemistry and Chemical Biology, Harvard University, 12 Oxford Street, Cambridge, Massachusetts 02138

ABSTRACT This paper examines the factors that influence the quality of nanostructures fabricated by sectioning thin films with an ultramicrotome ("nanoskiving"). It surveys different materials (metals, ceramics, semiconductors, and conjugated polymers), deposition techniques (evaporation, sputter deposition, electroless deposition, chemical-vapor deposition, solution-phase synthesis, and spin-coating), and geometries (nanowires or two-dimensional arrays of rings and crescents). It then correlates the extent of fragmentation of the nanostructures with the composition of the thin films, the methods used to deposit them, and the parameters used for sectioning. There are four major conclusions. (i) Films of soft and compliant metals (those that have bulk values of hardness less than or equal to those of palladium, or ≤500 MPa) tend to remain intact upon sectioning, whereas hard and stiff metals (those that have values of hardness greater than or equal to those of platinum, or ≥500 MPa) tend to fragment. (ii) All conjugated polymers tested form intact nanostructures. (iii) The extent of fragmentation is lowest when the direction of cutting is perpendicular to the exposed edge of the embedded film. (iv) The speed of cutting—from 0.1 to 8 mm/s—has no effect on the frequency of defects. Defects generated during sectioning include scoring from defects in the knife, delamination of the film from the matrix, and compression of the matrix. The materials tested were: aluminum, titanium, nickel, copper, palladium, silver, platinum, gold, lead, bismuth, germanium, silicon dioxide (SiO_2), alumina (Al_2O_3), tin-doped indium oxide (ITO), lead sulfide nanocrystals, the semiconducting polymers poly(2-methoxy-5-(2′-ethyl-hexyloxy)-1,4-phenylene vinylene) (MEH-PPV), poly(3-hexylthiophene) (P3HT), and poly(benzimidazobenzophenanthroline ladder) (BBL), and the conductive polymer poly(3,4-ethylenedioxythiophene):poly(styrenesulfonate) (PEDOT:PSS).

KEYWORDS: nanoskiving • nanofabrication • nanowires • microtome • ultramicrotomy • soft lithography

INTRODUCTION

This paper surveys materials for use in nanoskiving—a process of fabrication whose key step is sectioning planar or topographically patterned thin films with an ultramicrotome (Figure 1) (1, 2), and correlates their composition and method of deposition with the qualities of structures produced (e.g., morphology and extent of fragmentation). We examined two types of structures—long nanowires and two-dimensional (2D) arrays of circular or semicircular particles—formed by sectioning thin films for defects due to intrinsic mechanical properties of the materials (e.g., brittleness). We also explored the origin of defects due to artifacts of the sectioning process, and conclude that compression of the matrix, scoring due to chips in the edge of the knife, and delamination of the film from the matrix are the most important. Nanoskiving is useful for generating nanostructures for applications in electronics (3) and optics (4, 5), and has the potential to be used for manufacturing certain types of structures (e.g., nanowires and 2D arrays of nanostructures). The information in this paper will be useful to those concerned with designing processes for fabrication based on nanoskiving.

BACKGROUND

Unconventional Nanofabrication. "Nanofabrication" generates structures with sizes of ≤100 nm in at least one lateral dimension (6, 7). Most commercial nanofabrication takes place in the semiconductor industry, where the high-precision tools of electron-beam writing and photolithography dominate, and are likely to continue to do so for the foreseeable future (8, 9). Many new applications for nanostructures, particularly in photonics (10), chemical (11) and biological sensing (12, 13), materials for energy conversion and storage (14, 15), and organic electronic devices (16), require structures that are simpler, extend over larger areas, and are less expensive than integrated circuits. Fabricating devices on non-planar, mechanically compliant, or
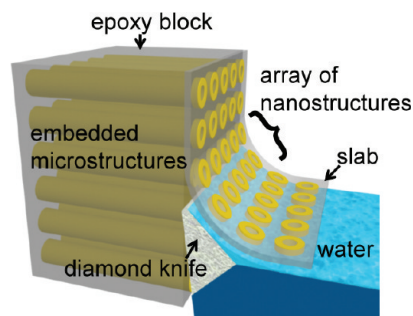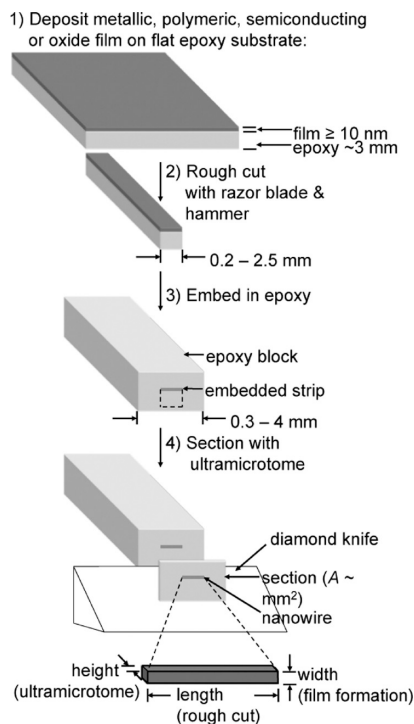

FIGURE 1. Schematic representation of the defining step of nanoskiving: mechanical sectioning of microfabricated structures with an ultramicrotome to replicate arrays of nanostructures embedded in thin polymeric slabs.

1) Deposit metallic, polymeric, semiconducting or oxide film on flat epoxy substrate:

film ≥ 10 nm
epoxy ~3 mm

2) Rough cut with razor blade & hammer

0.2 – 2.5 mm

3) Embed in epoxy

epoxy block
embedded strip
0.3 – 4 mm

4) Section with ultramicrotome

diamond knife
section (A ~ mm²)
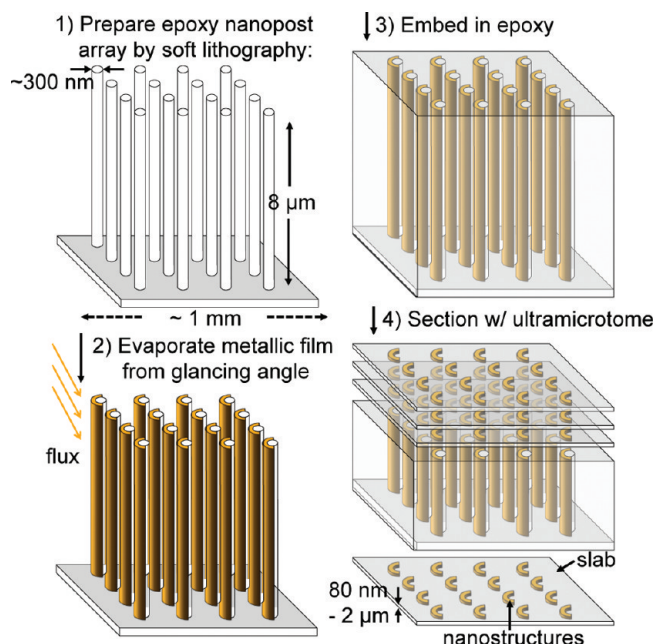nanowire

height (ultramicrotome)
length (rough cut)
width (film formation)

FIGURE 2. Summary of the process used for fabricating nanowires of loosely defined length (> 100 μm) by sectioning thin films. (1) A piece of flat epoxy served as the substrate for deposition of a metallic, polymeric, semiconducting, or oxide film. (2) A rough cut provided a strip of this film supported by epoxy, (3) which we embedded in additional epoxy. (4) Ultrathin sectioning (nanoskiving) and removal of the epoxy matrix formed nanowires in which each dimension was controlled by a different step of the process.

disposable substrates could lead to important applications that motivate the development of "unconventional" methods of nanofabrication (10). Soft lithographic printing and molding, and other methods, have begun to fill these niches in research laboratories, and are expected to play important roles in manufacturing in the future (7).

Nanoskiving. Nanoskiving is a technique for replicating nanostructures that substitutes "cutting" or "sectioning" for "printing" or "molding". The process builds on three well-established technologies: (i) methods of forming thin films (e.g., physical- and chemical-vapor deposition), (ii) patterning relief structures in polymers by molding (e.g., replica molding (17, 18) and nanoimprint lithography (19, 20), and (iii) using an ultramicrotome to cut thin sections from a block of polymer containing embedded nanostructures. There are two general strategies to form nanostructures by nanoskiving: sectioning perpendicular to a planar thin film and sectioning parallel to a pattern of relief structures coated conformally with a thin film (1).

The first process (Figure 2) produces nanowires (21). Stacking and sectioning multiple films, separated by sacrificial layers (e.g., polymers or SiO_2), which can be etched in a later step, can produce closely spaced parallel nanowires (22). Topographic patterning can introduce angles into these nanowires to form simple elements for nanoelectronics, such as parallel electrodes (3). Patterning the thin film into stripes, and sectioning perpendicular to the stripes, can produce nanowires with well-defined lengths and spacings

1) Prepare epoxy nanopost array by soft lithography:
~300 nm

8 μm

~ 1 mm

2) Evaporate metallic film from glancing angle
flux

3) Embed in epoxy

4) Section w/ ultramicrotome

80 nm - 2 μm
slab
nanostructures

FIGURE 3. Summary of the process used to generate two-dimensional arrays of metallic crescent-shaped nanoparticles. (1) Soft lithographic molding afforded an array of epoxy nanoposts. (2) Shadow evaporation, using a collimated source, deposited metal roughly halfway around the circumferences of the nanoposts. (3) Additional epoxy embedded the entire structure. (4) The ultramicrotome sectioned the embedded array into manipulable slabs containing arrays of metallic crescents.

(23). The second process (Figure 3) produces 2D arrays of nanostructures. The outlines of the molded features define the geometries of the structures produced by sectioning (5).

Ultramicrotomy. The microtome was invented in the 1770s to section specimens of wood for microscopy (24). Microtomy, the practice of generating thin sections for analysis, has since developed alongside microscopy (25). The invention of electron microscopy (EM) in the 1950s motivated the development of the ultramicrotome, an instrument that can section specimens into slabs <100 nm in thickness under ambient conditions (25). Ultramicrotomy is ubiquitous in histology and polymeric materials science. In the science of hard materials, it is a complement to the more common techniques for the preparation of samples of ion thinning and electropolishing (26). When equipped with a diamond knife, the ultramicrotome can section even hard materials. Examples include: industrial alumina (27); nanocrystalline pure elements, alloys, and ceramics (28); diamond films (29); steel sheets (30); and stacked layers of semiconductors (31).

Comparison of Nanoskiving with Materials Ultramicrotomy. Nanoskiving can be treated as ultramicrotomy of materials having the goal of generating functional nanostructures, rather than of preparing specimens for EM. There are at least four other important differences. (i) In materials ultramicrotomy, the embedded specimen is usually a bulk sample. In nanoskiving, the embedded specimen is usually a thin film. (ii) In materials ultramicrotomy, the requirement of transmission of electrons in EM imposes a limit on the thickness of sections to <100 nm. In nanoskiving, sections can be 30 nm to 10 μm thick, or greater. (iii) In
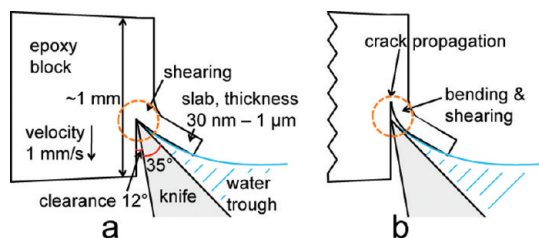
FIGURE 4. Schematic drawings of two mechanisms proposed for sectioning with an ultramicrotome. (a) In "true" or "shear" sectioning, the edge of the knife maintains contact with both the facet of the block and the underside of the epoxy slab. This mechanism produces a region of intense shearing, which is responsible for shear lamellae that are visible in micromachined chips of steel. This mechanism operates for metals and soft materials. (b) The mechanism of crack initiation and propagation is active for brittle materials, such as ceramics. The orange circle highlights the location within the sectioning process where the two models are different.

materials ultramicrotomy, small-area sections ($< 200~\mu$m in width) are easier to obtain than large-area sections, because the force per unit length exerted by the knife on the facet of a block is greater for small facets than for large facets, and because it is easier to maneuver a small facet to an unworn region of the knife (32). In nanoskiving, it is often desirable to fabricate arrays of nanostructures over as large an area as possible ($\geq 1~$mm^2). (iv) In materials ultramicrotomy, extensively fractured specimens of brittle materials or specimens damaged by artifacts of the sectioning process can yield fragments that are large enough for analysis. In nanoskiving, any fracturing can be catastrophic, and fracturing limits the materials that can be used. An understanding of the properties of materials that make them amenable to nanoskiving would enable it to be applied more broadly and rationally than it now is.

Mechanism of Sectioning. The ability of an ultramicrotome to cut thin sections (as thin as 30 nm) is astonishing (1). Sectioning involves a complicated interplay of processes: compression of the sample; tension perpendicular to the plane of sectioning; formation of new surfaces; bending, as the slab reorients from vertical to horizontal; shearing stress; friction of the slabs on the knife; and heat (33). There are two possible mechanisms for the sectioning process: (i) true, or shear, sectioning, in which the edge of the knife maintains intimate contact with both the facet of the block and the nascent slab (Figure 4a); and (ii) a mechanism of crack initiation and propagation, in which the knife splits or cleaves the block (Figure 4b). There is evidence for both processes, and each process can be present to different degrees in the same epoxy block, because each material within the block (or different grains or phases within the same material) can respond differently to the force of the knife (e.g., cleavage vs shattering).

Processes resembling true sectioning (Figure 4a) appear to dominate for metals and alloys (32). The shearing of the slab produces shear lamellae in the sections, perpendicular to the direction of cutting. Microtomed sections of aluminum (thickness = 500 nm) and micromachined chips of steel display this morphology, which is characteristic of unstable plastic flow in metals and alloys (32). The appearance of

scoring on both the top and bottom surfaces of slabs of some specimens also suggests a mechanism like that of Figure 4a (32).

Processes of crack initiation and propagation (Figure 4b) appear to operate for brittle materials such as minerals and ceramics (26). The knife initiates a crack, which follows the path of weakest molecular strength (34). Acetarin et al. argued in favor of some degree of crack propagation for all specimens because of the observation of craze formation (33) within slabs and also because it is impossible for a knife to be infinitely sharp; the radius of curvature of diamond knives is typically 3−6 nm, or a few tens of atoms (35). The extent to which crack propagation extends ahead of the knife edge depends on the amount of energy the sample can absorb by plastic flow prior to fracture (as in a measurement of hardness with a sharp indenter). Jésior postulated that the distance between the crack and knife increases with increasing hardness of the specimen. He argued that the farther the crack propagates ahead of the knife, the larger the radius over which the slab has to bend to go from vertical to horizontal, and thus the smaller the compressive stress on the slab while bending (34).

The orientation of cleavage planes in crystalline samples also determines the extent of fragmentation upon sectioning, as Antonovsky observed in samples of alumina (27). True sectioning and crack propagation can apparently operate at the same time on different grains within the same specimen. In samples of high-strength steel, Malis observed regions with shear lamellae, which are consistent with true sectioning (Figure 4a), as well as large defect-free regions, which is evidence of cleavage (Figure 4b) (32). Ultramicrotomes, when equipped with sensors, have also been used as analytical tools to measure fracture toughness and other properties of specimens (36).

Mechanical Properties of Thin Films. The ability to obtain intact nanostructures after sectioning depends on the mechanical properties of the film. These properties are strongly influenced by the morphology of the film, which depends on the technique used for deposition (37). In general, evaporated metallic films are polycrystalline and assume a columnar grain structure whose columns are perpendicular to the substrate (37). Evaporation of covalent solids, such as silicon and germanium, forms amorphous films (37). Evaporated films of oxides and nitrides can be depleted of oxygen and nitrogen. Compared to evaporation, sputtering-coating generally affords the user more control over the morphology of the thin film, and preserves the stoichiometry.

Evaporated metallic films can be up to 100 times harder and stronger more than their bulk, annealed counterparts (37). These polycrystalline films have two characteristics that are responsible for their hardness and strength. (i) Work hardening: high densities of dislocations (1×10^{10} to $1 \times 10^{12}~$cm^{-2}) correspond to those of extensively worked bulk metals. (ii) Grain-boundary strengthening: the sizes of grains in thin films (10−1000 nm) can be a few orders of magnitude smaller than those of bulk samples. Work hardening

and grain-boundary strengthening combine to produce films in which the mobilities of dislocations is impeded, plastic flow is restricted, and thus strength, hardness, and brittleness are increased (37).

Scope. There are no absolute criteria for the successful sectioning of materials by ultramicrotomy. This paper provides practical information for the selection of materials and processes of deposition. It also describes the artifacts that influence sectioning (and how to avoid them), and their influence on the nanostructures produced. For reviews of the practical aspects of ultramicrotomy, see Goldstein and Newbury (38); for a review of ultramicrotomy applied to the science of inorganic materials, see Malis and Steele (32); for a survey of embedding resins, see Acetarin et al. (33); for a perspective on the role of ultramicrotomy for biological applications, see Villiger (39); and for a history of ultramicrotomy, see Pease and Porter (25).

EXPERIMENTAL DESIGN

Selection of Thin-Film Materials. We sectioned films of several different materials, including metals, semiconductors, metal oxides, conjugated polymers (semiconducting and conducting), and films of semiconductor nanocrystals. The materials chosen occupy a range of different mechanical properties, and most have not been used with nanoskiving before.

Selection of Processes of Deposition. For metals, our primary method of deposition was electron-beam (e-beam) evaporation (40). We used sputter-deposition for films of platinum and ceramic materials, to try to control the amount of fragmentation in the nanostructures produced. We synthesized microplates ($d \approx 10-70$ μm) of single-crystalline gold (41), which we sectioned into nanowires. Electroless deposition provided amorphous films of nickel on epoxy substrates. We deposited ceramic films by evaporation, sputter deposition, or plasma-enhanced chemical-vapor deposition (PECVD). We deposited films of conjugated polymers and semiconductor nanocrystals by spin-coating and drop-casting. We deposited polypyrrole electrochemically.

Fabrication of Nanowires by Sectioning Thin Films. A stringent test that enabled us to determine the applicability of materials for nanoskiving was to form long nanowires (300 μm to 1 mm) by sectioning thin films, and to determine the extent of fragmentation by scanning electron microscopy (SEM). We measured electrical conductivity to verify the continuity of some of the nanowires. We used the process summarized in Figure 2 for all of these experiments. We sectioned the thin films with a direction of cutting perpendicular to the edge of the thin film. In this orientation, the action of the knife compressed the slab along the short axis of the nanowire. We also determined the effect of compression on the frequency of defects when the direction of cutting was parallel to the edge of embedded film for some metals.

Fabrication of 2D Arrays of Crescents and Rings by Sectioning Arrays of Nanoposts. We fabricated arrays of simple semicircular and circular structures using a process summarized in Figure 3, which began by forming an array of epoxy nanoposts by soft lithography (42). Line-of-sight deposition of metal on the sidewalls of these posts, followed by embedding, and sectioning with the ultramicrotome, produced metallic crescent-shaped nanostructures. Conformal coating by a sputtering process, followed by embedding and sectioning, produced arrays of rings. Examination of the structures produced by these processes provided (i) the yield of unbroken structures and (ii) the rate of compression of the axis of the array parallel to the direction of cutting.

Selection of Embedding Resin. An embedding resin should have (i) a relatively high value of elastic modulus (~3 GPa; a block that is too elastic deflects from the knife, rather than cleave), and (ii) a high yield stress after which the material undergoes plastic deformation (~70 MPa, otherwise the slab will deform upon sectioning) (33). Epoxy resins such as Epon, Araldite 502, and Epo-Fix (which is used for all experiments in this paper, unless otherwise noted) possess most of the properties required for good sectioning. Epo-Fix (Electron Microscopy Sciences) is a typical two-part epoxy containing polymers of bisphenol-A diglycidyl ether and triethylene tetraamine. It has excellent adhesion to most materials tested and can be cured at room temperature (the best results were achieved for 60° C for 2 h) from a prepolymer with relatively low viscosity (5 × 10^{-2} Pa s), which facilitates impregnation of porous samples. Epo-Fix is relatively hard (75 Shore D) (43) and stiff (flexural modulus = 2.4 GPa). Epo-Fix exhibits significant compression along the direction of cutting (15−20 % for 100 nm sections). This rate of compression ensured that the thin films would have to be sufficiently soft and compliant to accommodate the strain due to the compression of the embedding resin, and thus imposed a strict criterion for the success or failure of a given thin film.

The best commercially available embedding resins occupy a narrow range of values of hardness and stiffness (close to the values quoted for Epo-Fix). For systematic studies of the effects of the mechanical properties of embedding resins on their behavior in ultramicrotomy, see Acetarin et al. (33). Beyond selecting a resin on the basis of its mechanical properties, the mechanism of curing should be compatible with the composition and geometry of the embedded structure. For example, a UV-cured resin is incompatible with porous samples if there is no direct path for the light to reach the prepolymer in the pores. Additionally, the process of curing usually generates heat. We did not, however, observe any deleterious effects of the rise in temperature during curing, which was not great enough to affect any of the materials used in this study.

Ultramicrotome and Knife. We used a Leica Ultracut UCT equipped with a 35° diamond knife for all applications (Diatome Ultra 35°). We and others found less compression and delamination of films from the resin with 35° knives than with 45° knives (26).

RESULTS AND DISCUSSION

Fabrication of Nanowires by Sectioning Thin Metallic Films. We deposited, embedded, and sectioned a series of ten different metallic thin films by e-beam evaporation: aluminum, titanium, nickel, copper, palladium, silver, platinum, gold, lead, and bismuth. We deposited three additional films of these materials using different techniques-a polycrystalline film of platinum by sputter deposition, single-crystalline microplates of gold by growth from solution (41), and an amorphous film of nickel by electroless deposition. We deposited most films with a thickness of 50−100 nm, and sectioned them with a programmed thickness of 80 nm at a velocity of 1 mm/s, with a direction of cutting perpendicular to the exposed edge of the film. The substrate for deposition of films of silver, gold, palladium, and platinum was the polished surface of a silicon wafer. After deposition, we transferred the film to epoxy by puddle-casting an epoxy prepolymer, curing it, and peeling off the solid epoxy, along with the metallic film ("template stripping") (44, 45). This method produced very flat films (rms roughness <1 nm) on the surface templated by the silicon wafer (45). We deposited all other materials directly on the
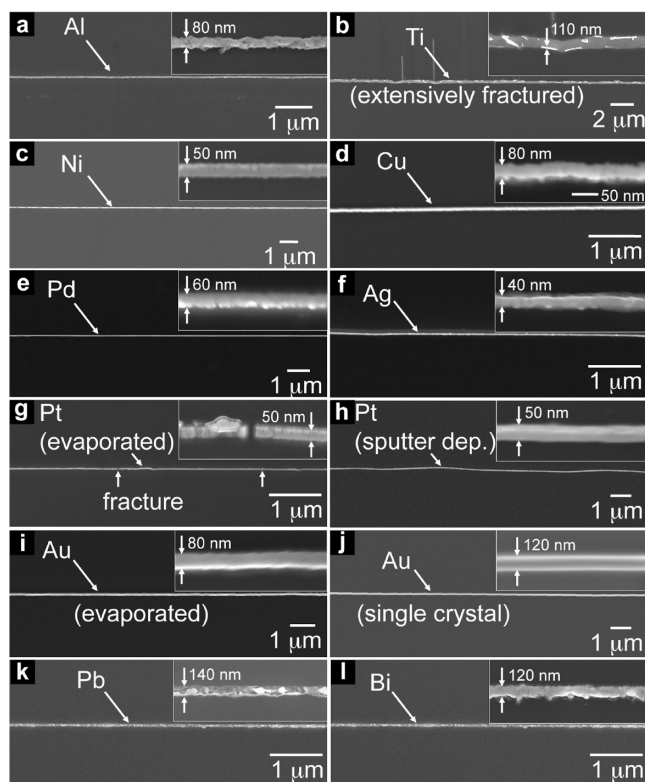
FIGURE 5. Scanning electron microscope (SEM) images of metallic nanowires formed by sectioning thin metallic films deposited by (a–g, i, k, l) electron-beam evaporation, (h) sputter deposition, and (j) solution-phase chemical growth. Metals are arranged by atomic mass. Soft and compliant materials—aluminum, copper, palladium, silver, gold, lead, and bismuth—formed long, intact nanowires over distances > 100 μm. Hard and rigid materials—titanium and platinum—tended to fracture. The epoxy surrounding the aluminum nanowire (a) was etched by an air plasma. The nanowire was likely converted, to some extent, to aluminum oxide. The titanium nanowire (b) is delaminated as well as extensively fractured. The arrows in the inset define the width of a fragment of the nanowire. The silicon substrate (light grey) is the thicker band running along the length of the image around the fragments of titanium.

flat side (rms roughness = 0.5 nm) of a cured epoxy substrate, prepared by puddle-casting the prepolymer against the polished side of a silicon wafer (4). Figure 5 shows representative spans of several of the nanowires produced by sectioning these films. Aluminum (5a), nickel (5c), copper (5d), palladium (5e), silver (5f), gold (5i), lead (5k), and bismuth (5l) formed nanowires with long unbroken spans, as determined by SEM. Most nanowires were 300 μm to 1 mm long. We defined this length loosely by cutting with a razor blade (see Figure 2, step 2). We attribute the roughness of some of the nanowires (e.g., bismuth) to the morphology of the thin film before sectioning.

Electrical Conductivity of Long Gold Nanowires.

To verify that inspection by SEM was an accurate method of determining physical continuity, we measured the electrical conductivity of the longest nanowires produced: a gold nanowire with dimensions of $l = 1.8$ mm, $w = 80$ nm, $h = 120$ nm. Figure 6 shows an SEM image and the electrical characteristics of a representative span of the nanowire. Based on these dimensions and the current at ±10 mV, we calculated a value of conductivity of 3.0×10^5 Ω^{-1} cm^{-1} (the
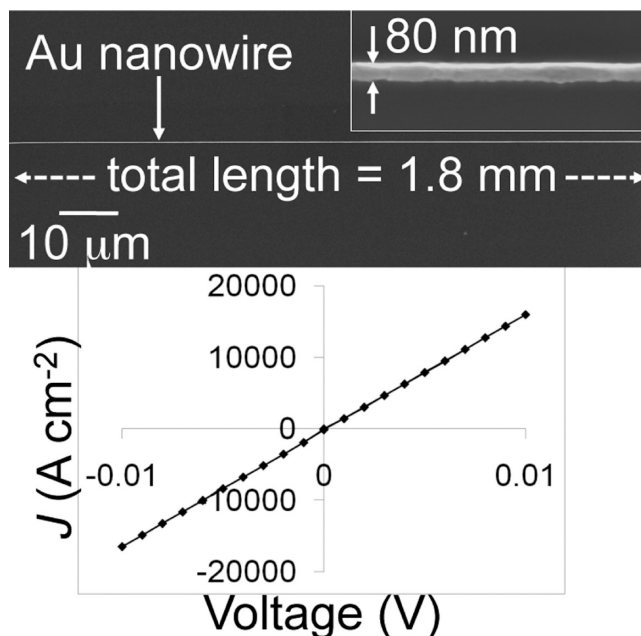
FIGURE 6. Scanning electron micrograph (top) of a long gold nanowire that was electrically continuous over a span of 1.8 mm. The plot (bottom) shows current density vs voltage of the nanowire across the span of 1.8 mm.

literature value for bulk gold is 4.5×10^5 Ω^{-1} cm^{-1}). We attribute the lower conductivity of the nanowire compared to that of bulk gold to thin regions of the nanowire where the true dimensions of the cross-section were smaller than the nominal height programmed by the ultramicrotome and the width set by the e-beam evaporator. Regions of constriction could be notches due to scoring by a damaged knife or thin spans caused by uneven evaporation of the thin film from which the nanowire was cut.

Correlation of Bulk Properties of Materials with Fragmentation of Thin Films.

Sectioning films of titanium (Figure 5b) and platinum (Figure 5g) produced fragmented nanowires. We verified, by SEM, that the films were intact prior to embedding and sectioning. In general, metals that formed intact nanowires upon sectioning were soft, compliant, and low-melting, based on values of bulk properties in the literature. Those that fragmented were hard, rigid, and high-melting. Metals as soft or softer than palladium—that is, metals with bulk values of hardness of the less than approximately 500 MPa (Vickers hardness number)—formed intact nanowires. The next hardest metal tested, platinum, broke into fragments with average lengths of 10 μm (Figure 5g). Evaporation of nickel produced an exceptionally resilient film by evaporation, which did not fragment. Titanium, the hardest material tested, fragmented extensively (Figure 5b).

Effect of Direction and Speed of Cutting on Fragmentation.

The orientation of an embedded thin film with respect to the direction of cutting had a profound effect on the frequency of defects and the morphology of the nanostructures that were formed. For example, sectioning with a direction of cutting perpendicular to the edge of an evaporated film of nickel formed unfragmented nanowires

(Figure 5c), whereas sectioning parallel to the edge of the same film produced fragmented nanowires whose segments had lengths of $10-20\,\mu$m. We attribute the higher frequency of defects in nanowires oriented parallel to the direction of cutting to compressive stress along the longitudinal axis of the nanowires. The breaks in the nanowires do not appear at regular intervals. This observation suggests that randomly located defects and thin areas (which arise from uneven chemical or physical vapor deposition) influence the sites of fracture. We define "fracture" as a break in the nanowire. Evaporated films of gold, palladium, nickel, and platinum, which displayed no or moderate fragmentation using a perpendicular direction of cutting, yielded fragments with lengths of approximately 100, 10, 10, and 1 μm, when sectioned parallel to the edge of the film.

In addition to increasing the rate of defects in the nanowires, a direction of cutting parallel to the edge of the film also imparted a roughened morphology to the nanowires. Pictures a and b in Figure 7 show the two relative orientations used in this paper between the direction of cutting and the edge of the embedded film: perpendicular (a) and parallel (b). Pictures c and d in Figure 7 show two palladium nanowires obtained from the same embedded film, but sectioned from orthogonal directions. The insets are close-up images that show the smooth microstructure of the film cut perpendicular to its edge (Figure 7c), and the rough microstructure of the nanowire cut parallel to its edge (Figure 7d). The rough microstructure in Figure 7d resembles the shear lamellae (parallel to the short axis of the nanowire) observed in microtomed foils of bulk metals (32).

Jésior published a series of papers on compression in ultramicrotomy, and how to avoid it (34, 46). He observed that the rate of compression of latex spheres was independent of the compression of the epoxy matrix. The soft latex spheres formed ellipses upon sectioning, and delaminated from the edges of the epoxy matrix (46). In our system, however, delamination of metallic films from the epoxy matrix was rare. Adhesion of metallic films to a compressible embedding resin (17% for 100-nm slabs of Epo-Fix) forces the nanowire to compress at the same rate as the matrix, and could be a factor responsible for the high rate of defects observed in hard and stiff films whose edges were oriented parallel to the direction of cutting.

Jésior also observed that compression is independent of the speed of cutting (34). Figure 7e shows a platinum nanowire oriented parallel to the direction of cutting using six speeds from $0.1-10$ mm/s. We found that the frequency of defects was independent of the speed of cutting, from $0.1-8$ mm/s. (The highest speed tested, 10 mm/s, actually decreased the frequency of defects. At this speed, the nanowire, and the surrounding epoxy, accommodated the compressive strain by buckling into long-range, wavelike distortions in the plane of the image. See Figure 7e, "10 mm/s".)

Fabrication of Platinum Nanowires from Sputter-Deposited Films.
Sputter-deposition can yield films with different morphologies: from polycrystalline metallic films
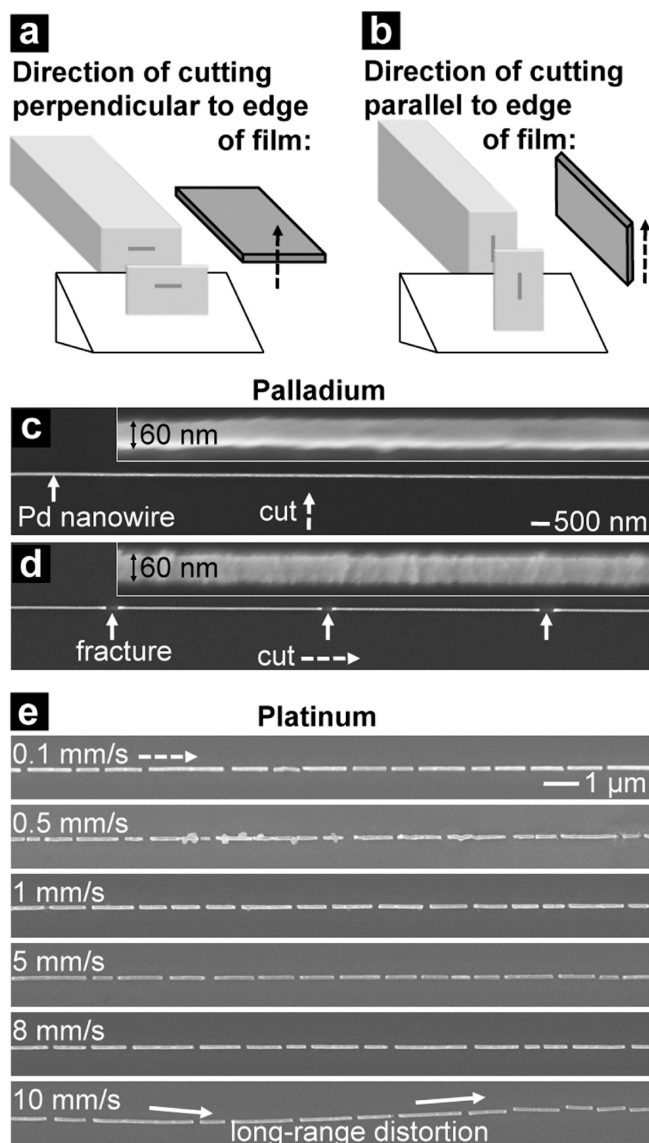
FIGURE 7. Effects of the direction of cutting on the morphology of nanostructures and the extent of fragmentation. (a) Palladium nanowire sectioned with the direction of cutting perpendicular to the edge of the film. (b) Nanowire sectioned with the direction of cutting parallel to the edge of the film. Sectioning parallel to the edge produces two effects: a rougher morphology (insets of a and b) and a higher frequency of fragmentation. (c) Effect of speed of sectioning on the frequency of fragmentation in platinum nanowires sectioned parallel to the plane of the film. There was no effect from 0.1 to 8 mm/s. With a speed of 10 mm/s, buckling accommodated some of the compressive strain and had the effect of reducing the frequency of defects.

with a range of mean grain size, to metallic glasses, and oxide films with stoichiometry that matches that of the source material (37). We found that a sputter-coated film of platinum was much more resistant to fracture than an evaporated film of the same thickness (50 nm, compare images g and h in Figure 5). While the evaporated film of platinum formed fragmented nanowires with 1 μm segments using a direction of cutting parallel to the edge of the film, the sputter-deposited film fragmented into 10 μm segments. We attribute the greater resilience of the sputtered film to morphological characteristics (density of dislocations

and the sizes of grains). We expect the parameters of deposition can be tuned to reduce the rate of fragmentation upon sectioning hard materials.

Fabrication of Gold Nanowires from Single-Crystalline Microplates. Polycrystalline films, deposited by physical vapor deposition, become polycrystalline nanostructures upon sectioning. Many applications however, require structures with smooth surfaces (e.g., metallic nanowires for plasmonic waveguiding) (47, 48). There is a family of procedures for the synthesis of single-crystalline metallic micro- and nanoparticles that provide control over the shapes and the compositions of these particles (49). Our laboratory previously reported the plasmonic properties of single-crystalline gold nanowires formed by nanoskiving single-crystalline microplates grown by solution-phase synthesis (4, 41). Observation of lattice fringes by TEM indicated that the crystallinity of the microplates was intact after sectioning. We have never observed fragmentation of single-crystalline gold nanowires, even those with lengths up to 50 μm (the longest we have produced). Comparing images i and j in Figure 5 illustrates the difference between polycrystalline and single-crystalline nanowires.

Fabrication of Nickel Nanowires from Amorphous Films. We also deposited and sectioned an amorphous nickel film by electroless deposition. Although this film formed an unfragmented nanowire with a direction of cutting perpendicular to the embedded film, it broke into fragments 500 nm to 1 μm long when cut with a parallel direction. These fragments were an order of magnitude smaller than those derived from the evaporated film of nickel. Correlation of the microstructures of the thin films, as determined by TEM, will be required to understand the extent to which morphology influences the extent of fragmentation.

Fabrication of Semiconductor Nanowires from Evaporated Films. Covalent solids, such as silicon and germanium, form amorphous films when evaporated. The most important result from the survey of polycrystalline metallic films was that soft materials form relatively soft thin films, which tend to form intact nanostructures upon sectioning. Initial results suggest that this generalization holds true for amorphous semiconductors, as well as for metals. We sectioned films of germanium and silicon using a direction of cutting perpendicular to the edge of the embedded thin film. The germanium film formed intact nanowires over lengths of >30 μm (Figure 8a), whereas the silicon film fractured extensively (Figure 8b).

Fabrication of Nanowires from Ceramic Films. Films of oxides, aluminum oxide (Al_2O_3), silicon dioxide (SiO_2), and tin-doped indium oxide (ITO), prepared by evaporation, sputter deposition, and PECVD, were the hardest materials we tested (Figure 8c−g). The only film that formed intact nanowires was a sputter-coated film of SiO_2. Applications that require long, intact spans of ceramic materials should be prepared using a softer material that can be converted to the film in its final form. For example, thermal oxidation and calcination can, in principle, convert
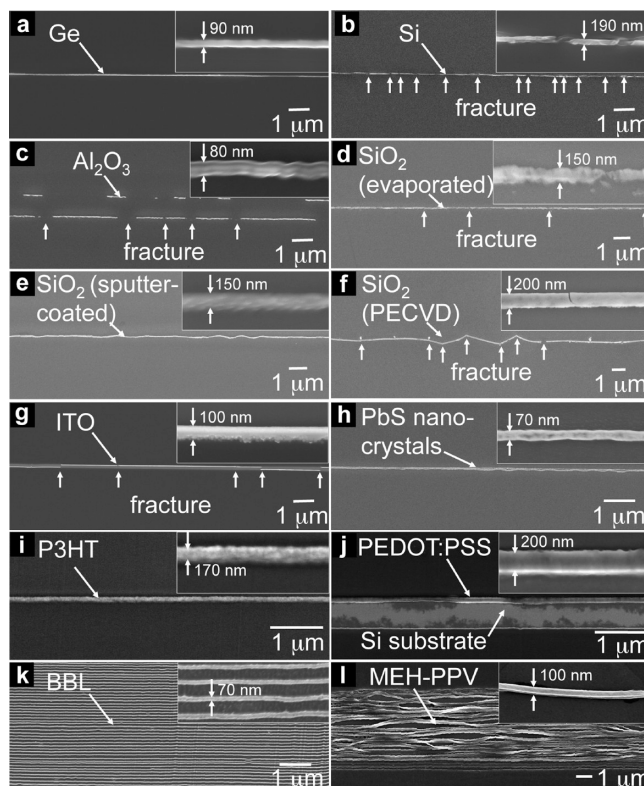
FIGURE 8. Nanowires of semiconductors, ceramics, and conjugated (semiconducting and conducting) polymers. All materials were deposited by e-beam evaporation unless otherwise noted. Among amorphous, evaporated elemental semiconductors, germanium remained intact (a), while silicon fragmented (b). All films of alumina and ITO deposited by evaporation (c and g) and sputter deposition (not shown) were fragmented. The film of alumina (c) delaminated from the epoxy matrix while it fractured. Extensive delamination and fracture produced two parallel strands with complementary fragments. The ability to form intact nanowires of SiO_2 depended strongly on the method used for deposition: sputter-deposited films remained intact, while evaporated films, and those deposited by plasma-enhanced chemical-vapor deposition (PECVD) fragmented. Spin-coated films of lead sulfide nanocrystals (h) formed intact nanowires, as did all conjugated polymer films tested (i−l). The single nanowire of PEDOT:PSS (j) adhered poorly to the epoxy matrix, but it did not fragment. The region labeled "Si substrate" is where the epoxy delaminated from the PEDOT:PSS during sectioning. Nanowires of BBL (k) and MEH-PPV (l) were made in groups of 50 by the procedure described in ref 22. The MEH-PPV nanowires tended to aggregate because of capillary forces during wet processing.

soft metallic films or sol−gel precursors, which section easily, into the desired ceramic materials (50).

Fabrication of Nanostructures of Solution-Processed Materials: Semiconductor Nanocrystals and Conjugated Polymers. Organic polymers and polymerlike materials are among the easiest materials to section with the ultramicrotome (22). Figure 8h is a nanowire derived from sectioning a spin-coated film of oleylamine-capped lead sulfide (PbS) nanocrystals (51), which formed long, intact segments. Figure 8i−l shows examples of conjugated (semiconducting and conducting) polymers: poly(3-hexylthiophene) (P3HT, Figure 8i), poly(3,4-ethylenedioxythiophene) poly-(styrenesulfonate) (PEDOT:PSS, Figure 8j), poly(benzimidazobenzophenantrholine ladder) (BBL, Figure 8k), and poly(2-methoxy-5-(2′-ethyl-hexyloxy)-1,4-phenylene vinylene) (MEH-

Table 1. Summary of the Materials, Methods of Deposition, and Average Intact Spans of the Nanowires Formed by Nanoskiving Thin Films

category	material	method of deposition	length of fragments (μm)
metals	Al	evaporation	unbroken
	Ti	evaporation	1 ($N=50$)
	Ni	evaporation	unbroken
	Ni	electroless deposition	unbroken
	Cu	evaporation	unbroken
	Pd	evaporation	unbroken
	Ag	evaporation	unbroken
	Pt	evaporation	10 ($N = 6$)
	Pt	sputter-deposition	unbroken
	Au	evaporation	unbroken
	Au	chemical growth	unbroken
	Pb	evaporation	unbroken
	Bi	evaporation	unbroken
semiconductors	Si	evaporation	5 ($N = 22$)
	Ge	evaporation	unbroken
oxides	SiO_2	evaporation	10 ($N=7$)
	SiO_2	sputter-deposition	unbroken
	SiO_2	PECVD	5 ($N = 16$)
	Al_2O_3	evaporation	1 ($N = 60$)
	Al_2O_3	sputter-deposition	4 ($N = 50$)
	ITO	evaporation	10 ($N = 5$)
	ITO	sputter-deposition	2 ($N = 60$)
polymers	P3HT	spin-coating	unbroken
	MEH-PPV	spin-coating	unbroken
	BBL	spin-coating	unbroken
	PEDOT:PSS	spin-coating	unbroken
nanocrystals	PbS	spin-coating	unbroken

PPV, Figure 8l). All of these materials formed intact nanowires regardless of the orientation of cutting.

Table 1 summarizes the materials, methods of deposition, and average intact spans of each nanowire produced by nanoskiving. We sectioned all films into slabs with a set thickness of 80 nm, using a direction of cutting normal to the plane of the film. We then inspected each nanowire by SEM. Nanowires fell into one of two categories: those that were unbroken, and those that broke into fragments with lengths of 1−10 μm. We determined the lengths of fragments for each material by obtaining an SEM image wide enough to determine the extent of fragmentation (the images had widths ≥30 μm near the centers of the nanowires) and divided the width of the image by the number of fragments (N). We did not analyze the distribution of the lengths of fragments statistically, but the sizes of fragments shown in Figures 5b and 8b−d, f, g are representative. For nanowires labeled "unbroken", we did not observe fragmentation along the entire lengths of nanowires, except at the termini, where the rough cut (Figure 1, step 2) fractured the film before embedding and sectioning.

Fabrication of 2D Arrays of Rings and Crescents. One of the most promising uses of nanoskiving is the fabrication and replication of 2D arrays of nanostructures embedded in thin slabs, which can be transferred to another substrate (52), for optics or other applications (5). Figure 3 summarizes the procedure used (53). Figure 9a shows an array of epoxy nanoposts, in which the sidewalls are partially coated with gold. Embedding these metalized posts in epoxy and sectioning parallel to the plane of the array produced 2D arrays of metallic nanostructures. The two most deleterious artifacts of mechanical sectioning that manifest themselves in 2D arrays formed by nanoskiving are (i) fracture of individual structures and (ii) compression of square arrays into rectangular arrays.

Yield of Intact Nanostructures in 2D Arrays. Figure 9b shows an array of platinum crescents. The yield of intact nanostructures was 93%. Of 320 crescents in the array shown, nine were broken in the center (see lower inset), and 13 were broken at the tips. Figure 9c shows counterfacing silver and silicon crescents patterned in the same plane. We did not find any broken structures in the array. The high yield (> 99%) of intact silicon crescents is unexpected, because the planar film of silicon, deposited using the same conditions of evaporation, was extensively fragmented when cut into a nanowire (see Figure 8b). A possible explanation is that small particles are not subject to long-range tensile stress that could contribute to fragmentation of nanowires. Table 2 summarizes the results of 2D arrays we have fabricated using previously published procedures (53). Silicon, palladium, silver, platinum, and gold crescents, and rings had wall thicknesses of 50−100 nm and outer diameters of ~350 nm. The polypyrrole was electrochemically deposited on a support of gold-coated epoxy nanoposts. When sectioned, the polypyrrole rings had wall thicknesses of ~400 nm and outer diameters of ~725 nm. The rings composed of lead sulfide nanocrystals had wall thicknesses of ~50 nm and diameters of ~1 μm.

Compression of 2D Arrays. The second effect of the sectioning process that is relevant to some applications is the compression of the array along the direction of cutting. We formed an array of gold crescents and measured the dimensions of the array and the angle between the axes (Figure 9d). The original array of posts, from which we cut this array of crescents, was square with a pitch of 2 μm between features. After sectioning (thickness =100 nm) using a randomly selected direction of cutting, we observed a shortening of both the vertical axis to 1.65 μm and the horizontal axis to 1.9 μm. We measured a direction of cutting of 73° from the horizontal row of crescents, as determined by a score, which was created by a defect in the knife and parallel to the direction of cutting. Because the direction of cutting was not parallel to either axis of the array, the compression skewed the array such that the unit cells deformed from square to diamond-shaped, with angles of 88.7 and 91.3°. The total compression in the direction of cutting was 17%. A survey of embedding resins led us to perform the same experiment with another epoxy, UVO-114 (a UV-curable resin obtained from Epoxy Technologies), and we measured 8% compression. (Through the course of the experiments described in this paper, and others, UVO-114 became our preferred resin for nanoskiving, in circumstances when it is possible to use a UV-cured resin.) In
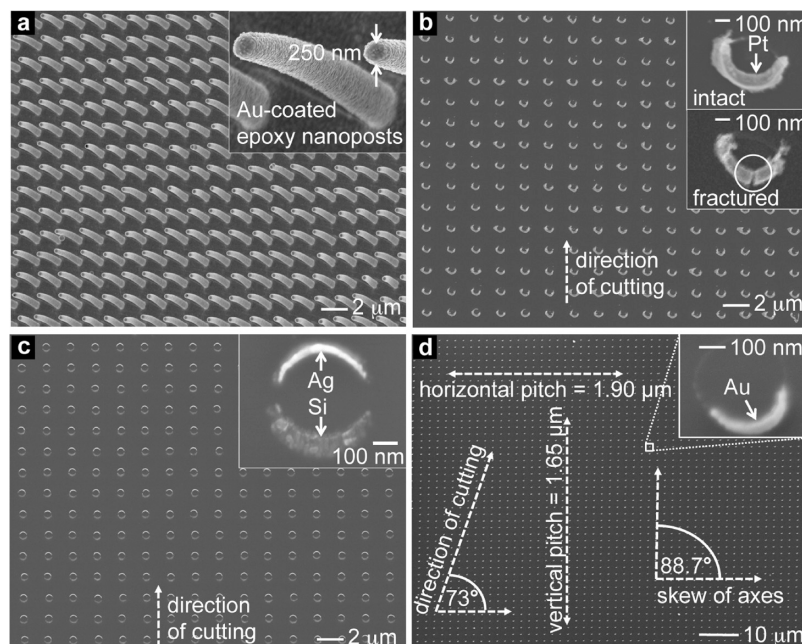
FIGURE 9. (a) Array of gold-coated epoxy nanoposts (the product of step 2, Figure 2). The posts are 8 μm tall, and 250 nm in diameter, at the top. (b) Array of platinum crescent-shaped nanoparticles. (c) Array of counterfacing crescents of silver and silicon. (d) Square array of nanostructures was compressed during the cutting operation.

Table 2. Table Summarizing the Materials, Methods of Deposition, Geometries, and Yields of Two-Dimensional Arrays of Nanostructures

material	method of deposition	geometry	yield (%)
Si	evaporation	crescents	>99.7
Pd	evaporation	crescents	>99.7
Ag	evaporation	crescents	>99.7
Pt	evaporation	crescents	93.1
Au	evaporation	crescents	99.9
Au	sputter-deposition	rings	>99.7
polypyrrole	electrodeposition	rings	>99.8
PbS nanocrystals	drop-casting	rings	97.5

general, the rate of compression decreases with thickness of the section and the hardness of the resin (34).

We summarized our findings and made predictions regarding the applicability of materials we have not yet tested in Figure 10. We assumed all metallic films were polycrystalline and all covalent solids were amorphous. Materials labeled "intact" are those that displayed no visible fragmentation, or large unbroken spans when cutting nanowires perpendicular to the plane of the embedded thin film. Films labeled "fragmented" fractured extensively into segments <10 μm. Those labeled "borderline" are films whose rate of fragmentation depended strongly on the method of deposition, the size and geometry of the structure (e.g., nanowires or crescents), and the orientation of the thin film with respect to the direction of cutting. We extrapolated our observations to make predictions for materials that we did not test, or for which we did not have enough data. In the case of relatively hard, d-block metals, our predictions are conservative; although we predict most would fragment, it might be possible to optimize the recipe for deposition to form films soft enough to promote a high yield of unfrag-

mented nanostructures. In the case of alkali and alkaline earth metals, we based our predictions on mechanical properties alone, and assumed that these films could be deposited and sectioned in an inert, dry environment. In addition to the materials in Tables 1 and 2, we sectioned chips (~10 μm thick) of highly oriented pyrolytic graphite. This material produced large intact spans of parallel plates when sectioned with a direction of cutting perpendicular to the edge of the chip; when sectioned parallel to the edge of the chip, the sample fractured extensively, into ~1 μm fragments. We thus labeled graphite as "borderline" in Figure 10.

Scoring. Chips in the edge of the diamond knife score the epoxy slabs and damage embedded structures in the paths of the scoring. A freshly sharpened knife contains no chips. As the knife is used, contact with hard material (commonly small inorganic dust particles from the laboratory, steel from the razor blade during trimming of the block face, or particularly hard samples) breaks microscopic pieces from the knife (32). These chips are inevitable, and knives must be re-sharpened after 6−12 months of normal use, at about half the cost of a new knife. Scoring was visible under dark-field optical microscopy, or by SEM (Figure 11a). Figure 11b shows a fracture caused by scoring in an aluminum nanowire. A region of delamination, where the silicon substrate is visible, accompanied the fracture. Scoring provides an exact marker of the direction of cutting on the surface of the epoxy slab and can be useful in distinguishing fractures due to a damaged knife from those due to the brittleness of the thin films.

Delamination. Adhesion of an embedded film to the epoxy matrix provides stability to the nanostructures during the process of sectioning. Distortion caused by delamination
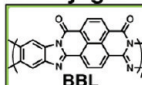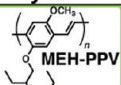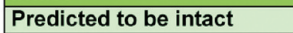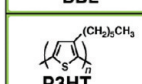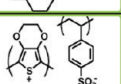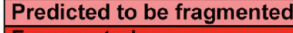
FIGURE 10. Summary of findings and predictions regarding the abilities of elements, oxides, polymers, and nanocrystals to form nanowires by sectioning thin films.

of the films from the epoxy matrix can impose tensile stress on nanostructures. The structures have higher tendencies to break in regions of delamination than in regions in which the matrix supports the embedded film on all sides. We observed the least amount of delamination by embedding freshly deposited films. Films that were exposed to the ambient atmosphere for several days tended to delaminate upon sectioning because of physisorption of adventitious organic material from the ambient air. A brief ($\sim$5 s) exposure to an air plasma removed adventitious organic material from metals such as gold, which would not be oxidized by plasma. Figure 11c shows a delaminated region in an epoxy slab containing a nickel nanowire. The delaminated regions extend for several micrometers, and contained the only fracturing we observed.

Chatter. Chatter is another artifact of ultramicrotomy, in which vibrations in the room or generated by friction between the knife and the sample produce parallel lines in the slab parallel to the edge of the knife. The effect is exacerbated when the knife is not securely fixed in the chuck. We rarely observed instances of chatter in these experiments, and direct the interested reader to the review by Malis and Steele for a discussion of this effect (32).

Oscillating Knives. We expected that ultrasonic, oscillating knives would produce better results than those obtained using stationary knives: Studer and Gnaegi have demonstrated that polystyrene blocks, sectioned with a 45° knife oscillating at 2 kHz with 400 nm amplitude, produced sections compressed by only 3.5 % (54). We found that, in addition to reducing compression, oscillating knives also produced nanostructures of higher quality than did stationary knives. Panels d and e in Figure 11 show gold nanowires cut with a knife without and with oscillation, using the frequency (2 kHz) and amplitude (400 nm) used by Studer and Gnaegi (54). The morphology and the edges of the nanowire are smoother if the knife is oscillated.

CONCLUSIONS

This paper surveyed several materials and processes of thin-film deposition, many of which had not been used with nanoskiving before. From this survey of materials and methods, we found a simple correlation between the propensities of thin evaporated metallic films to fragment, and their bulk values of hardness. The materials that yielded intact nanostructures upon sectioning tended to be soft. Understanding the exact relationship between the morphology of thin films (including surface oxides), their mechanical properties, and their performance in nanoskiving will require further experimentation (e.g., a combination of analysis using TEM, and measurements of the indentation hardness or tensile strength of the thin films). We predict, however, that the rate of defects observed by microtoming thin films would agree qualitatively with measurements of mechanical properties. We also determined the effects of other parameters, such as the orientation of cutting with respect to the embedded thin films, the condition of the diamond knife, and the adhesion of the thin film to the matrix. These experiments provide a practical model for selecting materials, methods of thin-film deposition, and parameters of sectioning for nanoskiving.

This paper also described factors that could limit the extent to which nanoskiving can be integrated with other techniques. Compression, for example, limits precise registration of arrays with structures produced by conventional lithography and with other arrays produced by nanoskiving. The effect of scoring is more pernicious, particularly if nanoskiving is to be used for production. The effect of accumulated damage to the edge of the knife if used continuously is unknown, but it would require resharpening of knives more frequently than is required for sectioning routine biological or inorganic materials. Complete avoidance of hard, inorganic particles requires samples to be molded, coated, and sectioned with assiduous attention to cleanliness (or, alternatively, require these steps to be
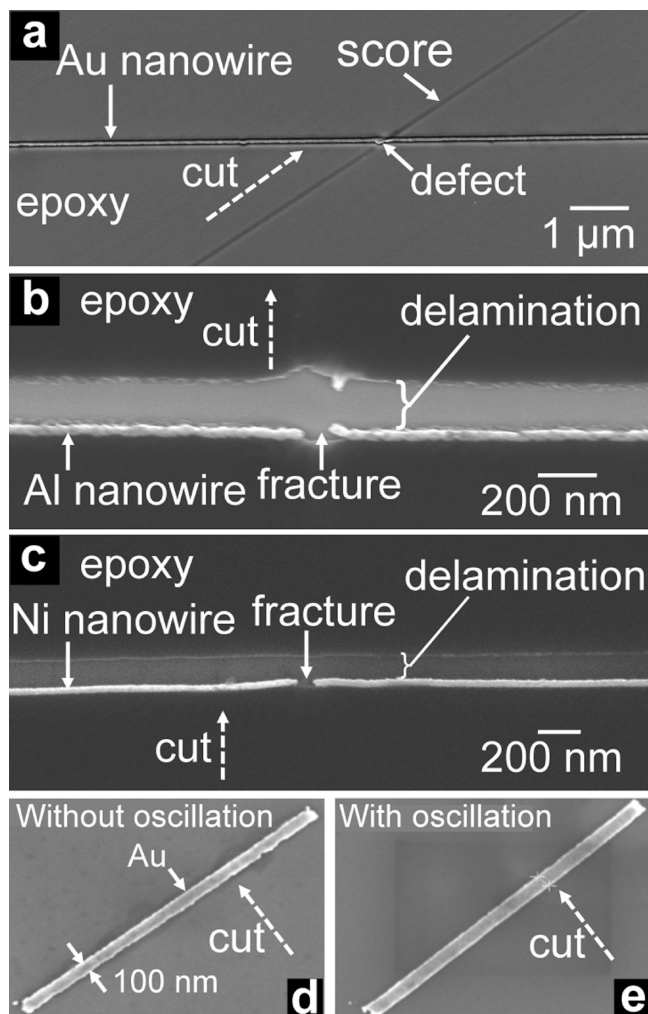
FIGURE 11. Examples of artifacts of the process of sectioning that are deleterious to the structures produced. (a) Divot in the edge of the knife produced the score on the surface of the epoxy matrix. The score damaged the gold nanowire at the point of intersection. (b) Defect in an aluminum nanowire and concomitant delamination of the nanowire from the epoxy matrix. The silicon support used for imaging by SEM is visible in the gap. (c) Poor adhesion of a nickel film to the epoxy matrix caused delamination of the nanowire from the slab. Delamination caused both sides of the nanowire to be supported unevenly during cutting, and the nanowire broke. (d) Image of a gold nanowire sectioned with a knife, without supersonic oscillation. (e) Nanowire cut from the same film with oscillation. The morphology and the roughness of the nanowire cut with oscillation are smoother than the nanowire cut using a stationary knife.

performed in a cleanroom). Despite these shortcomings, nanoskiving is still among the most general methods of fabricating nanostructures with respect to different classes of materials, and is possibly the only method that can pattern multiple materials in the same plane in a single step (as in Figure 9b).

There could be opportunities to exploit what we called "artifacts" in this paper to fabricate structures that cannot be made easily with other methods. For example, controlled fragmentation of nanowires produces nanogaps, which could be used to concentrate electric fields (55); deliberate scoring using knives with engineered defects could be used for perforation of nanostructures for the same purpose; and compression and skewing of 2D arrays of nanostructures

could be used to generate anisotropic arrays using an isotropic master (42).

Nanoskiving is the first technique to use mechanical sectioning as the key step in the fabrication and replication of nanostructures singly or in arrays. This report should be useful as nanoskiving develops and for designing other processes of nanomachining in the future.

METHODS

Materials. We obtained Epo-Fix embedding resin from Electron Microscopy Sciences, and UVO-114 from Epoxy Technology, Inc. We obtained metals for evaporation from the Kurt J. Lesker Company. All other chemicals were purchased from Sigma Aldrich. We deposited almost all metals directly onto planar epoxy substrates, which we prepared by mixing Epo-Fix in a ratio (v:v) of base to hardener of 7.5:1 in a sealed centrifuge tube by shaking. We degassed the prepolymer in a vacuum desiccator. We then poured the prepolymer over the polished side of a silicon wafer (we contained the liquid prepolymer using a ring of PDMS) and cured the epoxy for 60 °C for 2 h. After cooling the epoxy to room temperature, we peeled the epoxy off the silicon using a razor blade. The surface of the epoxy had a value of roughness (rms) of 0.5 nm (as determined by AFM). To promote adhesion of the thin films to the epoxy substrate, we treated the surface of the epoxy with an air plasma (100 W, 1 Torr, 30 s). All films except those of gold, silver, palladium, and platinum were deposited on freshly plasma-treated epoxy substrates.

The smoothest films of gold, silver, palladium, and platinum were prepared by template stripping (45). In this procedure, the film was evaporated on a silicon wafer and peeled off by curing epoxy against the evaporated film.

Electron-Beam Evaporation. We evaporated films with in a chamber with a base pressure of 1×10^{-6} Torr, an accelerating voltage of 10 kV, a filament current of 0.6−1 A, and rates of deposition of ~1 Å/s for all materials. The substrate was placed 40 cm above the source.

Sputter Deposition. We sputter-deposited films of platinum, aluminum oxide, ITO, and silicon dioxide using an AJA model ATC sputtering system, which operated at a base pressure of 8×10^{-7} Torr. We introduced argon into the chamber at a rate of 40 sccm/s. The pressure during deposition was 4 mtorr. The platinum film was deposited at 450 V (DC) at 50 % power, with a rate of deposition of 3.6 Å/s. The aluminum oxide film was deposited at 198 V (RF) at 50 % power, with a rate of deposition of 0.1 Å/s. The ITO film was deposited at 198 V (RF) at 50 % power, with a rate of deposition of 0.6 Å/s. The silicon dioxide film was deposited at 450 V (DC) at 50 % power, with a rate of 0.12 Å/s.

PECVD. We deposited a film of silicon dioxide by PECVD using a Surface Technology Systems (STS) system operating at a base pressure of 1.2×10^{-5} Torr and a pressure of 4 mtorr during deposition. DC power (475 V) and RF power (150 V) were running simultaneously during the deposition.

Spin-Coating of Conjugated Polymer Films. We deposited films of P3HT, and BBL and MEH-PPV, were deposited by spin-coating using previously described conditions (22, 52). We deposited films of PEDOT:PSS from a 0.65 % dispersion in water (by diluting a 1.3 % dispersion as obtained from Aldrich) by spin-coating at a rate of 1 krpm and annealing in a vacuum oven at 125 °C for 2 h. We prepared a solution of lead sulfide nanocrystals in hexanes by a reported procedure at a concentration of approximately 1×10^{16} nanocrystals/L (56). Spin-coating this solution onto an epoxy substrate (1 krpm), followed by a 1 s exposure to air plasma (100 W, 500 mtorr), provided a mechanically resilient 100 nm thick film of nanocrystals.

Embedding. We cut the metallic, semiconducting, ceramic, and polymeric films, supported by their epoxy substrates, into

strips, ~5 mm long, and 0.3−1 mm long. We placed these strips in polyethylene embedding molds (Electron Microscopy Sciences), filled the molds with mixed and degassed Epo-Fix prepolymer, and cured the blocks at 60 °C for 2 h.

Ultramicrotomy. We sectioned all films with a Leica Ultracut UCT ultramicrotome equipped with a Diatome Ultra 35° diamond knife with a 6° built-in clearance angle. An additional, external 6° clearance angle produced a total cutting angle of 47°. We cut all slabs using a cutting speed of 1 mm/s and a programmed thickness of 80 or 100 nm. The Supporting Information of the paper by Xu et al. (5) contains a description of the cutting process.

REFERENCES AND NOTES

(1) Xu, Q. B.; Rioux, R. M.; Dickey, M. D.; Whitesides, G. M. *Acc. Chem. Res.* **2008**, *41*, 1566−1577.

(2) Xu, Q.; Rioux, R. M.; Whitesides, G. M. *ACS Nano* **2007**, *1*, 215−227.

(3) Dickey, M. D.; Lipomi, D. J.; Bracher, P. J.; Whitesides, G. M. *Nano Lett.* **2008**, *8*, 4568−4573.

(4) Wiley, B. J.; Lipomi, D. I.; Bao, J. M.; Capasso, F.; Whitesides, G. M. *Nano Lett.* **2008**, *8*, 3023−3028.

(5) Xu, Q. B.; Bao, J. M.; Rioux, R. M.; Perez-Castillejos, R.; Capasso, F.; Whitesides, G. M. *Nano Lett.* **2007**, *7*, 2800−2805.

(6) Gates, B. D.; Xu, Q. B.; Stewart, M.; Ryan, D.; Willson, C. G.; Whitesides, G. M. *Chem. Rev.* **2005**, *105*, 1171−1196.

(7) Stewart, M. E. M., M. J.; Yao, J.; Thompson, L. B.; Nuzzo, R. B. *Proc. IMechE Part N: J. Nanoeng. Nanosyst.* **2007**, *220*, 81−138.

(8) Willson, C. G.; Roman, B. J. *ACS Nano* **2008**, *2*, 1323−1328.

(9) Pease, R. F.; Chou, S. Y. *Proc. IEEE* **2008**, *96*, 248−270.

(10) Stewart, M. E.; Anderton, C. R.; Thompson, L. B.; Maria, J.; Gray, S. K.; Rogers, J. A.; Nuzzo, R. G. *Chem. Rev.* **2008**, *108*, 494−521.

(11) Yun, M. H.; Myung, N. V.; Vasquez, R. P.; Lee, C. S.; Menke, E.; Penner, R. M. *Nano Lett.* **2004**, *4*, 419−422.

(12) Cui, Y.; Wei, Q. Q.; Park, H. K.; Lieber, C. M. *Science* **2001**, *293*, 1289−1292.

(13) Ramanathan, K.; Bangar, M. A.; Yun, M.; Chen, W.; Myung, N. V.; Mulchandani, A. *J. Am. Chem. Soc.* **2005**, *127*, 496−497.

(14) Boettcher, S. W.; Spurgeon, J. M.; Putnam, M. C.; Warren, E. L.; Turner-Evans, D. B.; Kelzenberg, M. D.; Maiolo, J. R.; Atwater, H. A.; Lewis, N. S. *Science* **2010**, *327*, 185−187.

(15) Williams, S. S.; Hampton, M. J.; Gowrishankar, V.; Ding, I. K.; Templeton, J. L.; Samulski, E. T.; DeSimone, J. M.; McGehee, M. D. *Chem. Mater.* **2008**, *20*, 5229−5234.

(16) Menard, E.; Meitl, M. A.; Sun, Y. G.; Park, J. U.; Shir, D. J. L.; Nam, Y. S.; Jeon, S.; Rogers, J. A. *Chem. Rev.* **2007**, *107*, 1117−1160.

(17) Xia, Y. N.; McClelland, J. J.; Gupta, R.; Qin, D.; Zhao, X. M.; Sohn, L. L.; Celotta, R. J.; Whitesides, G. M. *Adv. Mater.* **1997**, *9*, 147−149.

(18) Xia, Y. N.; Kim, E.; Zhao, X. M.; Rogers, J. A.; Prentiss, M.; Whitesides, G. M. *Science* **1996**, *273*, 347−349.

(19) Chou, S. Y.; Krauss, P. R.; Renstrom, P. J. *J. Vac. Sci. Technol., B* **1996**, *14*, 4129−4133.

(20) Willson, C. G. *J. Photopolym. Sci. Technol.* **2009**, *22*, 147−153.

(21) Xu, Q. B.; Gates, B. D.; Whitesides, G. M. *J. Am. Chem. Soc.* **2004**, *126*, 1332−1333.

(22) Lipomi, D. J.; Chiechi, R. C.; Dickey, M. D.; Whitesides, G. M. *Nano Lett.* **2008**, *8*, 2100−2105.

(23) Xu, Q. B.; Bao, J. M.; Capasso, F.; Whitesides, G. M. *Angew. Chem., Int. Ed.* **2006**, *45*, 3631−3635.

(24) Hill, J. *The Construction of Timber*; Imperial Academy: London, 1770.

(25) Pease, D. C.; Porter, K. R. *J. Cell Biol.* **1981**, *91*, S287−S292.

(26) Malis, T. *Microsc. Res. Technol.* **1995**, *31*, 265−266.

(27) Antonovsky, A. *Microsc. Res. Technol.* **1995**, *31*, 300−307.

(28) McMahon, G.; Malis, T. *Microsc. Res. Technol.* **1995**, *31*, 267−274.

(29) Swab, P. *Microsc. Res. Technol.* **1995**, *31*, 308−310.

(30) Barreto, M. P.; Veillette, R.; Lesperance, G. *Microsc. Res. Technol.* **1995**, *31*, 293−299.

(31) Glanvill, S. R. *Microsc. Res. Technol.* **1995**, *31*, 275−284.

(32) Malis, T. F.; Steele, D. *Mater. Res. Soc. Symp. Proc.* **1990**, *199*, 3−50.

(33) Acetarin, J. D.; Carlemalm, E.; Kellenberger, E.; Villiger, W. *J. Electron Microsc. Technol.* **1987**, *6*, 63−79.

(34) Jesior, J. C. *Ultrastruct. Mol. Struct. Res.* **1986**, *95*, 210−217.

(35) Matzelle, T. R.; Gnaegi, H.; Ricker, A.; Reichelt, R. *J. Microsc. Oxford* **2003**, *209*, 113−117.

(36) Atkins, A. G.; Vincent, J. F. V. *J. Mater. Sci. Lett.* **1984**, *3*, 310−312.

(37) Ohring, M. *Materials Science of Thin Films, Deposition and Structure*, 2nd ed.; Academic Press: San Diego, CA, 2002.

(38) Goldstein, J.; Newbury, D. E.; Joy, D. C.; Lyman, C.; Echlin, P.; Lifshin, C. E.; Sawyer, L.; Michael, J. R. *Scanning Electron Microscopy and X-Ray Analysis* 3rd ed.; Springer: New York, 2003.

(39) Villiger, W.; Bremer, A. *J. Struct. Biol.* **1990**, *104*, 178−188.

(40) Graper, E. B. *J. Vac. Sci. Technol., A* **1987**, *5*, 2718−2723.

(41) Kan, C. X.; Zhu, X. G.; Wang, G. H. *J. Phys. Chem. B* **2006**, *110*, 4651−4656.

(42) Pokroy, B.; Epstein, A. K.; Persson-Gulda, M. C. M.; Aizenberg, J. *Adv. Mater.* **2009**, *21*, 463−469.

(43) Technical Data Sheet: Epo-fix Cold-Setting Embedding Resin. http://www.emsdiasum.com/microscopy/technical/datasheet/1232.aspx (accessed March 28, 2010).

(44) Nagpal, P.; Lindquist, N. C.; Oh, S. H.; Norris, D. J. *Science* **2009**, *325*, 594−597.

(45) Weiss, E. A.; Kaufman, G. K.; Kriebel, J. K.; Li, Z.; Schalek, R.; Whitesides, G. M. *Langmuir* **2007**, *23*, 9686−9694.

(46) Jesior, J. C. *J. Ultrastruct. Res.* **1985**, *90*, 135−144.

(47) Ditlbacher, H.; Hohenau, A.; Wagner, D.; Kreibig, U.; Rogers, M.; Hofer, F.; Aussenegg, F. R.; Krenn, J. R. *Phys. Rev. Lett.* **2005**, *95*, 257403.

(48) Pyayt, A. L.; Wiley, B.; Xia, Y. N.; Chen, A.; Dalton, L. *Nat. Nanotechnol.* **2008**, *3*, 660−665.

(49) Xia, Y.; Xiong, Y. J.; Lim, B.; Skrabalak, S. E. *Angew. Chem., Int. Ed.* **2009**, *48*, 60−103.

(50) Choi, S. Y.; Mamak, M.; Coombs, N.; Chopra, N.; Ozin, G. A. *Adv. Funct. Mater.* **2004**, *14*, 335−344.

(51) Cademartiri, L.; von Freymann, G.; Arsenault, A. C.; Bertolotti, J.; Wiersma, D. S.; Kitaev, V.; Ozin, G. A. *Small* **2005**, *1*, 1184−1187.

(52) Lipomi, D. J.; Ilievski, F.; Wiley, B. J.; Deotare, P. B.; Loncar, M.; Whitesides, G. M. *ACS Nano* **2009**, *3*, 3315−3325.

(53) Lipomi, D. J.; Kats, M. A.; Kim, P.; Kang, S. H.; Aizenberg, J.; Capasso, F.; Whitesides, G. M. *ACS Nano* **2010**, *4*, 4017−4026.

(54) Studer, D.; Gnaegi, H. *J. Microsc. Oxford* **2000**, *197*, 94−100.

(55) Cubukcu, E.; Yu, N. F.; Smythe, E. J.; Diehl, L.; Crozier, K. B.; Capasso, F. *IEEE J. Sel. Top. Quantum Electron.* **2008**, *14*, 1448−1461.

(56) Ghadimi, A.; Cademartiri, L.; Kamp, U.; Ozin, G. A. *Nano Lett.* **2007**, *7*, 3864−3868.

AM100434G